Emergence of broadband variability in a marine plankton model under external forcing

Benjamin Mayersohn, Marina Lévy, Inès Mangolte, K. Shafer Smith

Figure 1.

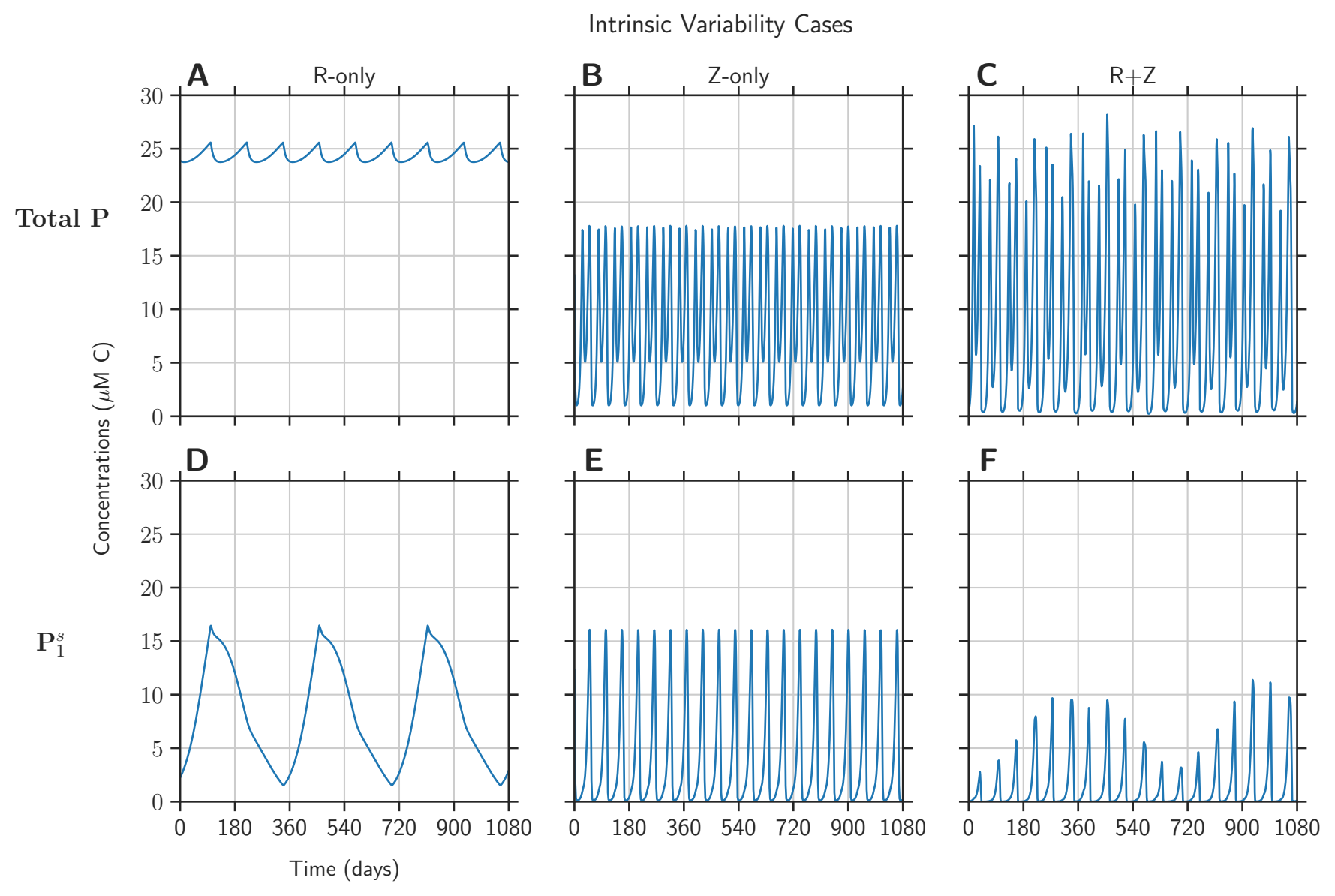
Intrinsic Variability Cases
A
R-only
B
Z-only
C
R+Z
D
E
F
Total P
P_1^s
Concentrations (μM C)
0
5
10
15
20
25
30
0
180
360
540
720
900
1080
Time (days)

Figure 2.

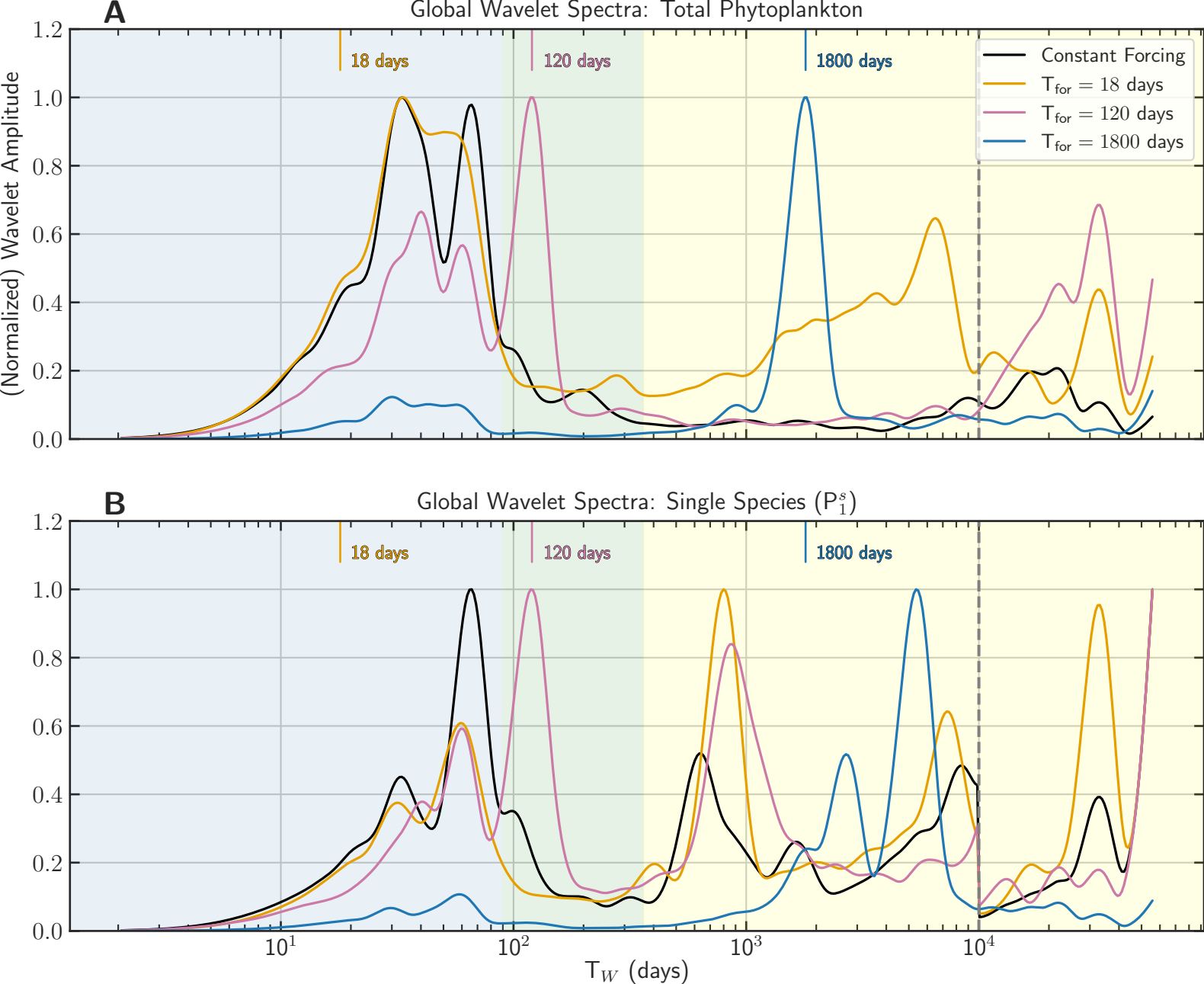
A
Global Wavelet Spectra: Total Phytoplankton
(Normalized) Wavelet Amplitude
18 days
120 days
1800 days
Constant Forcing
$T_{for} = 18$ days
$T_{for} = 120$ days
$T_{for} = 1800$ days
B
Global Wavelet Spectra: Single Species (P_1^s)
T_W (days)

Figure 3.

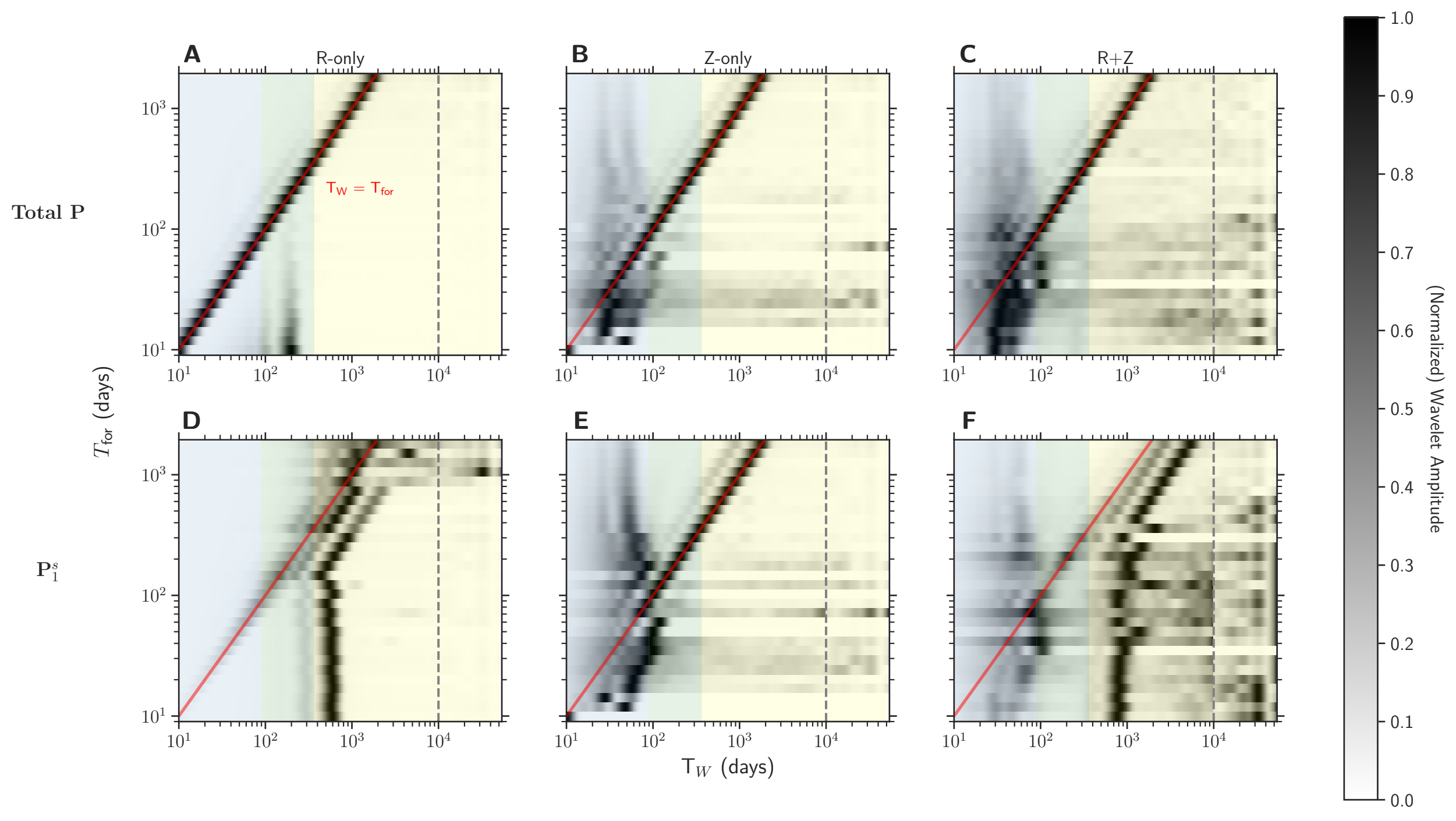
A
R-only
B
Z-only
C
R+Z
D
E
F
Total P
$\mathbf{P}_1^s$
T_{for} (days)
T_W (days)
$T_W = T_{for}$
10^1
10^2
10^3
10^4
1.0
0.9
0.8
0.7
0.6
0.5
0.4
0.3
0.2
0.1
0.0
(Normalized) Wavelet Amplitude

Figure 4.

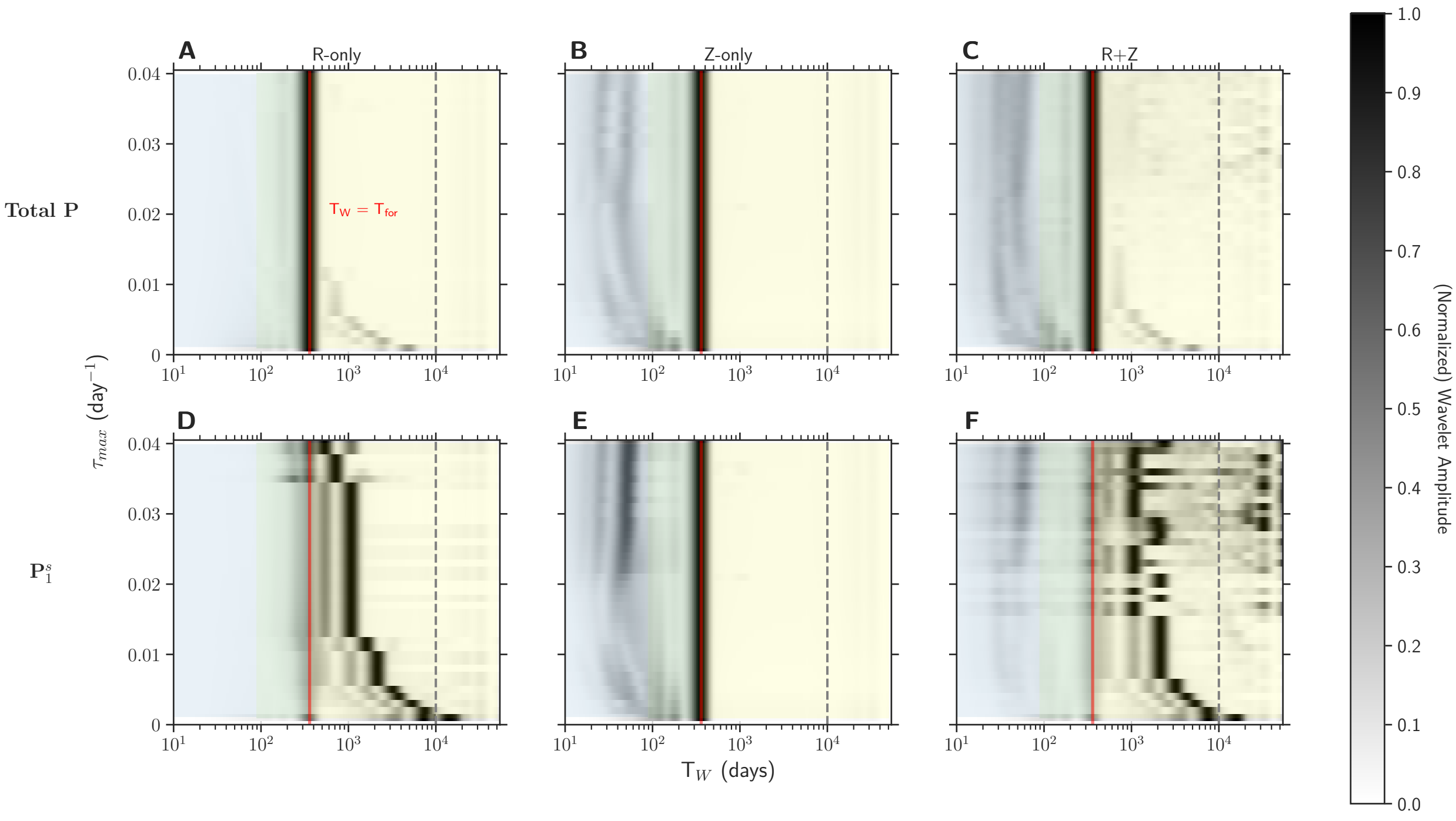
A
R-only
B
Z-only
C
R+Z
D
E
F
Total P
P_1^s
$T_W = T_{for}$
τ_{max} (day^{-1})
T_W (days)
(Normalized) Wavelet Amplitude
0.04
0.03
0.02
0.01
0
10^1
10^2
10^3
10^4
1.0
0.9
0.8
0.7
0.6
0.5
0.4
0.3
0.2
0.1
0.0

Figure 5.

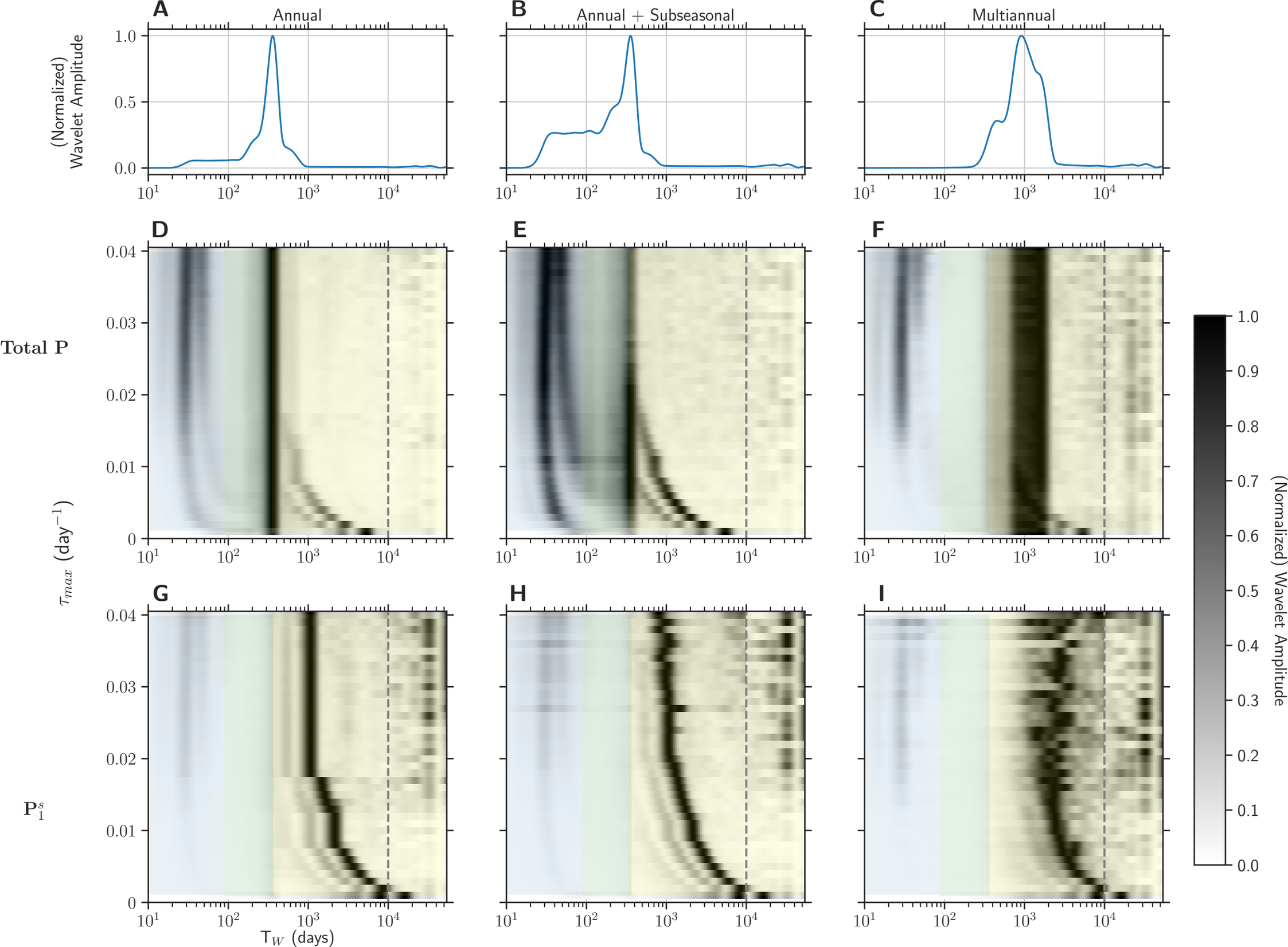
A
Annual
B
Annual + Subseasonal
C
Multiannual
(Normalized)
Wavelet Amplitude
1.0
0.5
0.0
10^1
10^2
10^3
10^4
D
E
F
G
H
I
Total P
$\mathbf{P}_1^s$
τ_{max} (day^{-1})
0.04
0.03
0.02
0.01
0
T_W (days)
(Normalized) Wavelet Amplitude
1.0
0.9
0.8
0.7
0.6
0.5
0.4
0.3
0.2
0.1
0.0

Figure 6.

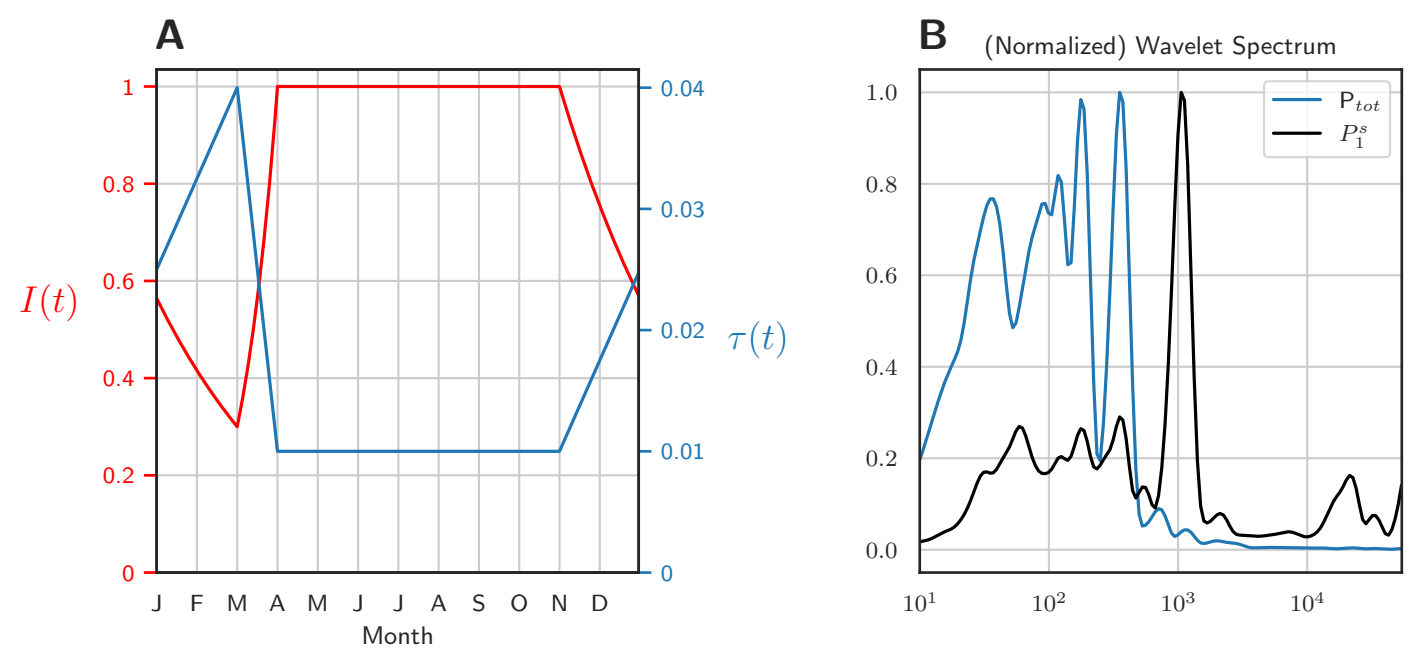
A
1
0.8
0.6
0.4
0.2
0
$I(t)$
0.04
0.03
0.02
0.01
0
$\tau(t)$
J F M A M J J A S O N D
Month
B
(Normalized) Wavelet Spectrum
1.0
0.8
0.6
0.4
0.2
0.0
P_{tot}
P_1^s
10^1
10^2
10^3
10^4

Emergence of broadband variability in a marine plankton model under external forcing

Benjamin Mayersohn[1], Marina Lévy[2,3], Inès Mangolte[3], K. Shafer Smith[1,2]

[1]Courant Institute of Mathematical Sciences, New York University, New York, New York 10012, USA
[2]Center for Prototype Climate Modeling, New York University, Abu Dhabi, UAE
[3]Sorbonne Université (CNRS/IRD/MNHN), Laboratoire d'Océanographie et du Climat (LOCEAN), Institut Pierre, Simon Laplace (IPSL), Paris Cedex 05 75252, France

Key Points:

- Phytoplankton respond to nutrient fluctuations with a wider frequency range than the forcing contains
- This is due to interactions between ecological and physical sources of variability
- The results are robust to a wide range of external nutrient fluctuations

Corresponding author: K. Shafer Smith, `kss3@nyu.edu`

Abstract

Temporal variability in plankton community structure and biomass is often driven by environmental fluctuations: nutrient supplies, light, stratification and temperature. But plankton time series also exhibit variability that is not strongly correlated with key physical variables and is distinctly nonlinear in nature. There is evidence, from both laboratory and modeling studies, that oscillations can arise from ecological interactions alone. In the open ocean, it is challenging to establish the roles and relative importance of environmental versus intrinsic processes in generating the observed ecological variability. To explore this competition, we employ a marine plankton model that supports two mechanisms of intrinsic ecological variability operating at distinct frequencies: predator-prey interactions between zooplankton and phytoplankton, with timescales of weeks, and resource competition that occurs with multiple nutrients phytoplankton species, with timescales of years. The model is forced by imposing variable nutrient input rates. representing typical open ocean situations, with periods ranging from subseasonal to multi-annual. We find that intrinsically-driven variability generally persists in the presence of extrinsic forcing, and that the interaction between the two can produce variability at frequencies that are not characteristic of either source. The intrinsic frequencies are found to be even more energetic when the extrinsic variability is augmented with stochastic noise. We conclude that interactions between intrinsic and extrinsic sources of variability may contribute to the wide range of observed frequencies in phytoplankton time series, and may explain why it is often difficult to relate planktonic variation to environmental variation alone.

Plain Language Summary

Phytoplankton play an important role in the oceanic carbon cycle, and providing nutrition to larger species in the oceanic food chain. For these reasons, it is important to understand the factors that drive variability in their abundance. There is often an (understandable) focus on physical drivers of variability, as phytoplankton are often subject to drastic changes in their environment. But phytoplankton communities also grow and shrink in size depending on the abundance of predators and the local abundance of particular nutrients. We are interested in understanding how environmental and ecological processes interact to shape time fluctuations in phytoplankton communities. By constructing an ecological model and subjecting it to nutrient fluctuations, we find that each kind of process leaves a distinct imprint on the emerging ecosystem dynamics. We conclude that one particular factor that influences a phytoplanktonic community will not necessarily overwhelm the others, and that there should be an emphasis on tailoring both physical and ecosystem models to accurately project changes in the face of climate change.

1 Introduction

At any given place in the ocean, phytoplankton exhibit complex changes in biomass and community composition over a variety of timescales. It is important to understand exactly what drives this natural variability in order to identify any ecological changes that may be attributed to anthropogenic factors. Ocean color observations of chlorophyll-a — a proxy for phytoplankton biomass — in the epipelagic zone indicate the presence of intraseasonal (weeks to months), seasonal, and interannual variability (Behrenfeld et al., 2006; Martinez et al., 2009; Resplandy et al., 2009; Vantrepotte & Mélin, 2011; Thomalla et al., 2011; Demarcq et al., 2012; Mayot et al., 2017; Salgado-Hernanz et al., 2019; Keerthi et al., 2020; Huisman et al., 2006). Abundances of phytoplankton functional types derived from ocean color remote sensing data suggest that community structure varies over a similar range of time scales (Alvain et al., 2008; D'Ovidio et al., 2010; Demarcq et al., 2012; Rousseaux & Gregg, 2015; Mayot et al., 2017; Dakos et al., 2009). This broad range of observed frequencies in phytoplankton communities is also seen in global biogeochemical models of the ocean (Aumont et al., 2018; Dutkiewicz et al., 2019).

Many of these patterns of variability can be attributed to specific physical processes in their environment. Annual blooms in phytoplankton biomass correlate with a variety of seasonal factors (Lévy, 2015) such as the shoaling of the mixed layer (Sverdrup, 1953), a reduction of turbulent mixing (Huisman et al., 1999), and a shutdown of atmospheric cooling (Taylor & Ferrari, 2011). Subseasonal variability is associated with basin-scale climate modes such as the Madden-Julian oscillation (Resplandy et al., 2009), atmospheric forcing via storms (Fauchereau et al., 2011; Carranza & Gille, 2014) and tropical cyclones (Menkes et al., 2016), and oceanic mesoscale and submesoscale processes (Mahadevan et al., 2012; Lévy et al., 2018; Poggiale et al., 2013; Keerthi et al., 2020). And interannual oscillations are explained by large-scale climate modes such as the El Niño-Southern Oscillation, Pacific Decadal Oscillation, and Atlantic Multidecadal Oscillation (Chavez et al., 2011).

However, there is evidence from laboratory data that variability can also emerge from ecological interactions. Predator-prey oscillations between phytoplankton and zooplankton have been observed to persist in a laboratory environment (Blasius et al., 2019; Hastings, 2020). Benincà et al. (2008) conducted a multiyear laboratory mesocosm experiment where the constituent functional groups fluctuated with periodicities ranging from 15 days to 225 days due to various food web interactions. Thus, while physical processes likely explain much of the observed variability in phytoplankton time series, ecological contributions cannot be entirely discounted.

Furthermore, observations of phytoplankton variability do not always neatly align with that of the dominant physical phenomena. For example, the annual spring bloom has wide variations in timing, amplitude, and ecological diversity (Smayda, 1998; Harris & Baxter, 1996; Talling, 1993). While this variability is often associated with annual variations in mixed layer shoaling and a seasonal reduction in turbulence, Dakos et al. (2009) have hypothesized — and demonstrated with their own ecosystem model — that intrinsic variability can interact with seasonal forcings to produce these interannual variations. There is supporting evidence for this hypothesis from empirical dynamical modeling (EDM) studies that show phytoplankton time series may be generated by dynamical systems that are inherently nonlinear and even chaotic in nature (Sugihara & May, 1990). In an EDM study by Hsieh et al. (2005), the authors demonstrated that time series of physical variables such as sea surface temperatures and climate indices in the North Pacific exhibited linear stochasticity, while ecological variables such as diatoms, fish and copepods showed signs of a low-dimensional nonlinearity. This could potentially explain why interannual variability can emerge in ecosystems even under seasonal forcings.

Disentangling the physical (extrinsic) and ecological (intrinsic) drivers of phytoplankton variability is difficult in observational data, but much can be learned from a modeling approach. Mayersohn et al. (2021) developed an intermediate-complexity chemostat-like ecosystem model with six phytoplankton species, two zooplankton species, and three nutrients. In the presence of steady external forcing, the model exhibits two distinct mechanisms of intrinsic variability: oscillations driven by differences in stoichiometry and the nutrient uptake curves between competing species (termed *R-oscillations*), and predator-prey interactions between zooplankton and phytoplankton (termed *Z-oscillations*). R-oscillations are characterized by response frequencies on the order of years, and are expressed as community structure variability with nearly constant net phytoplankton biomass. Z-oscillations occur on faster timescales, of order weeks to months, and generate variability in total biomass. When both mechanisms are active and interacting, community structure varies as well. Each mechanism can be suppressed (e.g. Z-oscillations can be omitted by turning off the zooplankton compartments), and when both are present, the response can be broadband and complex, and yet still exhibit a spectral gap between the two responses.

In the present paper, we make use of the same model, and examine how this emerging variability is affected when external conditions are varied in time, and consider the

following questions: if the system is subjected to time-varying external forcings with dominant frequencies that differ from the frequencies that emerge from intrinsic processes, which frequencies will emerge in the phytoplankton populations? Will the external frequencies dictate the behavior of the ecosystem and wash away any previously-existing intrinsic variability? Will the interactions between the different sources of variability produce frequencies that are uncharacteristic of either? Does this potentially explain misalignments between observed variability in chlorophyll and the dominant physical drivers of variability? We consider first periodic external conditions with frequencies ranging from days to years, and then explore more realistic external forcings with noise and broadband forcing.

In section 2, we present and explain the model equations, including the numerical model and analysis methods used for our experiments. Section 3 considers the effects of single-band periodic forcings, with a range of forcing periods and maximum dilution rates, and section 4 considers more realistic broadband, stochastic forcings. Section 5 considers the effect of light limitation and nutrient supply, varying together in a manner reflective of an idealized North Atlantic bloom scenario. Section 6 expands upon and summarizes the results of the aforementioned sections, and suggests some additional lines of investigation that could be pursued in future work.

2 Ecosystem model

We summarize here our chemostat-like ecosystem model (Mayersohn et al., 2021; Mayersohn & Mangolte, 2022), which was developed to have the minimum complexity necessary to capture the essence of full fledged biogeochemical components of an Earth system model (e.g. PISCES, Aumont et al., 2015), while still being tractable. The model includes six phytoplankton species, three small (P_1^s through P_3^s) and three large (P_1^l through P_3^l). Two grazers — one microzooplankton (Z^s) and one mesozooplankton (Z^l) — are also included: Z^s exclusively consumes small phytoplankton, while Z^l is an omnivore that consumes Z^s and the large phytoplankton. The model includes three dissolved inorganic resource compartments R_j, representative of nitrogen (R_1, μM N), phosphorus (R_2, μM PO_4), and iron (R_3, μM Fe). Phytoplankton and zooplankton compartments have units of μM C, with stoichiometric conversions for the phytoplankton compartments described in Mayersohn et al. (2021). The model simulates a chemostat setting, where each nutrient R_j is relaxed toward its target value S_j at a dilution rate τ that can be held constant or varied in time. Phytoplankton and zooplankton are removed from the system through natural mortality and also via an outflow at the dilution rate τ. Explicit remineralization and gravitational export are omitted. While the model lacks a detrital compartment, prior studies show that predator-prey cycles can persist in models that do have explicit remineralization (Edwards, 2001), and oscillations driven by competition for resources have been observed in planktonic mesocosm experiments with heterotrophic bacteria (Heerkloss & Klinkenberg, 1998). Thus, we choose to omit a detrital compartment for simplicity. Phytoplankton mortality is linear, while zooplankton mortality is quadratic to parameterize density-dependent losses such as viral infection, as well as unrepresented trophic levels (Aumont et al., 2015). In most of our experiments light and temperature are kept constant in time.

The equations are

$$\frac{dR_j}{dt} = \tau(t)\left(S_j - R_j\right) - \sum_{i=1}^{3} C_{ji}\left[\mu^s \min_j \frac{R_j}{K^s_{ji}+R_j} P^s_i + \mu^l \min_j \frac{R_j}{K^l_{ji}+R_j} P^l_i\right], \quad (1a)$$

$$\frac{dP^s_i}{dt} = -\tau(t)P^s_i + \left[\mu^s \min_j \frac{R_j}{K^s_{ji}+R_j} - m_P - \frac{g^s Z^s}{K_Z + P^s_{\text{tot}}}\right] P^s_i, \quad (1b)$$

$$\frac{dP^l_i}{dt} = -\tau(t)P^l_i + \left[\mu^l \min_j \frac{R_j}{K^l_{ji}+R_j} - m_P - \frac{g^l Z^l}{K_Z + Z^s + P^l_{\text{tot}}}\right] P^l_i, \quad (1c)$$

$$\frac{dZ^s}{dt} = -\tau(t)Z^s + \frac{g^s Z^s}{K_Z + P^s_{\text{tot}}} P^s_{\text{tot}} - \left[\frac{g^l Z^l}{K_Z + Z^s + P^l_{\text{tot}}} + m_Z Z^s\right] Z^s, \quad (1d)$$

$$\frac{dZ^l}{dt} = -\tau(t)Z^l + \frac{g^l Z^l}{K_Z + Z^s + P^l_{\text{tot}}}\left(Z^s + P^l_{\text{tot}}\right) - m_Z (Z^l)^2, \quad (1e)$$

where $i, j = 1, 2, 3$, and $P^{s,l}_{\text{tot}} = \sum_{i=1}^{3} P^{s,l}_i$. The values of the model parameters are presented in Mayersohn et al. (2021) and repeated in Table 1. The parameters C_{ji} and $K^{s,l}_{ji}$ denote the stoichiometric composition and nutrient limitation of each phytoplankton with respect to nutrient R_j. These parameters control the rate and existence of R-oscillations, which we summarize below. The grazing terms, which are proportional to a maximum grazing rate $g^{s,l}$, control the rate and existence of Z-oscillations. Mayersohn et al. (2021) uses two configurations for the maximum grazing rate: a weak predation configuration $(g^s, g^l = 1.5, 0.5)$, and a strong predation configuration that scales these values by 1.15. In this study, we use the strong predation configuration to explore a full range of dynamic possibilities (chaotic interactions were not present in the weak predation configuration).

Numerical model and analysis method

All simulations presented are run for 200 years, with each year containing 360 days, and the last 150 years of each simulation used for analysis. This long analysis timespan is chosen not because of the spinup time (which is typically a few years), but because some simulations exhibit periods on the order of decades, or even aperiodic behavior. All simulations are integrated in time using the SciPy `odeint` library (Millman & Aivazis, 2011), with the model written in Python 3.9.

In most plots, we consider the total biomass of the six phytoplankton species, and the biomass of a single species; because all six phytoplankton species have similar time variability, we show results for only one of them, P^s_1. We include the individual phytoplankton because it gives us a sense of how the evolution of an single functional type would affect the community composition over time.

The time-averaged, or *global* wavelet spectra were computed using the `waipy` library, which relies on the work of Torrence and Compo (1998). We use the Morlet wavelet with a wavenumber of 6. The resolved periods of the spectrum (octaves) are represented by powers of 2, with 32 suboctaves per octave. In other words, for $j = 0, 1, 2, \ldots$ such that $2^{1+j/32} \leq 54000$,

$$W_j = 2^{1+j/32} \text{ days}. \quad (2)$$

This gives us 471 resolved periods $T_W = \{W_0, \ldots, W_{470}\}$ (T_W will be used from here on to refer to periods in the wavelet spectrum.)

While the continuous wavelet transform results in a function of both time and frequency, we only use the time-averaged wavelet spectra. We have chosen this method over the more common Fourier transform because of the aperiodic nature of the phytoplankton time series. Fourier spectra tend to be especially broadband and noisy due to the wide variety of frequencies present in the ecosystem. In contrast, the global wavelet spectra are smooth and easier to interpret.

Fundamental modes of internal variability

When $\tau(t)$ is held constant Mayersohn et al. (2021) showed that intrinsic variability can occur via two distinct mechanisms:

R-oscillations: Differences in stoichiometry and nutrient limitation between competing species drive an oscillation in a system with at least three nutrients and three phytoplankton species (Tilman, 1985; Huisman & Weissing, 1999). Suppose at a given time that P_1 is most abundant, so that it removes the nutrient for which it has the greatest stoichiometric need at the fastest rate. A competitor, say P_2, that is least limited by this depleted nutrient then grows rapidly, overtaking P_1, setting up an analogous scenario for P_3 to invade, and so on, in an endless cycle of rock-paper-scissors. With the parameters used in our model, these oscillations tend to occur with frequencies on the order of months for the total phytoplankton and years for the individual phytoplankton. This oscillation can be suppressed by keeping only one small and one large species of phytoplankton.

Z-oscillations: In systems with zooplankton and phytoplankton, predator-prey cycles emerge, with or without the presence of multiple nutrients. In our model, microzooplankton control small phytoplankton from the top down, but are limited in growth by mesozooplankton, whereas mesozooplankton graze on large phytoplankton and are limited only by the quadratic mortality term. Microzooplankton are therefore somewhat restricted in growth, typically confined to short bursts following a bloom in their prey. These oscillations are faster than R-oscillations, and typically have frequencies on the order of months for both the total and individual phytoplankton. This oscillation can be suppressed by omitting the zooplankton species.

To summarize the findings of Mayersohn et al. (2021) and to provide a constant-forcing reference case, Figure 1 shows the time variability for the total and individual phytoplankton for three cases under constant forcing: *R-only*, which omits zooplankton species to allow only R-oscillations; *Z-only*, which keeps only one large and one small phytoplankton species, thereby admitting only Z-oscillations; and *R+Z*, which corresponds to the strong predation case in Mayersohn et al. (2021). Panel F of Figure 1, which shows the individual phytoplankton P_1^s in the *R+Z* case, can be seen as a combination of the dominant modes of P_1^s exhibited in panels D (*R-only*) and E (*Z-only*).

3 Periodic forcing

We first consider a range of single-band periodic forcings, imposing sinusoidal variation on the dilution rate $\tau(t)$, with forcing periods ranging between 10 and 1800 days. The periods are chosen in order to cover sub-seasonal nutrient supplies in response to events such as storms or eddies, seasonal fluctuations in nutrient delivery due to seasonally varying entrainment or upwelling, and interannual fluctuations associated with El Niño or the Southern Annular Model. The forcing also varies in maximum amplitude to represent different efficiencies in nutrient supplies, and in minimum amplitude to account for periods with little or no nutrient supply. The variable dilution rate takes the form

$$\tau(t) = \frac{1}{2}\left[\tau_{\max} + \tau_{\min} + (\tau_{\max} - \tau_{\min}) \sin\left(\frac{2\pi t}{T_{\text{for}}}\right)\right], \tag{3}$$

where $\tau_{\min}$ and $\tau_{\max}$ are the minimum and maximum dilution rates, respectively, and T_{for} is the forcing period.

Figure 2 shows the wavelet spectra of the total phytoplankton (A) and an individual phytoplankton P_1^s (B) in the *R+Z* scenario under constant forcing and sinusoidal forcing periods $T_{\text{for}} = 18, 120$, and 1800 days. For the constant forcing scenario, we see two dominant subseasonal peaks in the total phytoplankton; these are the Z-oscillations, and

most of the variability is contained there. The individual small phytoplankton also exhibit Z-oscillations in the same frequency range, one of the peaks is more dominant than the other. R-oscillations, which appear as a bump at roughly 600 days, are present in the individual phytoplankton but not the total. We can clearly see that the individual phytoplankton have a much more broadband spectrum than the total, with visible energy over a broad range of frequencies. Furthermore, for the individual phytoplankton, the constant forcing scenario achieves a maximum value at the longest wavelet (i.e. the length of the analysis window), which is strong indicator of aperiodicity in the system. In general, the presence of significant broadband low frequency energy in the spectrum implies an irregular peak structure in the time series, which is likely chaotic or quasiperiodic.

When the external variability has a short period of 18 days, the emerging variability in the total phytoplankton occurs on a broad spectrum, with a wide region of low frequency energy not present in the constant forcing scenario. At 120 days, there is some degree of phase locking: the frequency of the forcing is dominant in the emerging phytoplankton spectra for both the total and individual series. At 1800 days, the Z-oscillations persist as well in both series. The Z-oscillations exhibit a diminished representation in the spectrum as the forcing period increases, but this is an effect of averaging the wavelet representation over the time domain to obtain the global wavelet spectrum; the Z-oscillations are suppressed whenever the external forcing reaches low values of τ, and the length of these oligotrophic time spans increases with the period of the external forcing. But the Z-oscillations are still active during the eutrophic (large τ) time spans. Therefore, the high frequency variability in both the individual and total phytoplankton is preserved.

Figure 3 presents stacked wavelet spectra of total phytoplankton (upper row) and P_1^s (lower row) for a range of forcing periods T_{for} (see caption). The three columns correspond to *R-only* (left), *Z-only* (middle) and *R+Z* (right) cases. In the *R-only* case, total phytoplankton shows a degree of phase-locking for all forcing periods, indicated by the alignment between the wavelet period T_{W} and the forcing period T_{for}. For the scenarios with Z-oscillations (panels B and C), the extrinsic forcing begins to have a visible impact on the emerging frequencies in total phytoplankton when the forcing period exceeds 30 days. But the high-frequency Z-oscillations persist across the full span of forcing periods. For the *R+Z* simulations (panel C), the R-oscillations seen in panel A are nowhere to be found. This is not surprising, as R-oscillations are primarily fluctuations in individual species, while Z-oscillations are biomass fluctuations. In addition, for external forcings ranging from roughly 10 to 120 days, low frequencies emerge that are not characteristic of either the intrinsic or extrinsic sources of variability.

For the single phytoplankton species P_1^s in the *R-only* case, the R-oscillations are dominant when the forcing frequency is high. Once the forcing period exceeds a threshold of roughly 200 days, the emerging dominant period of the phytoplankton becomes proportional to the forcing period. The forcing period thus controls the rate of species succession. When the forcing period exceeds 1000 days, a bifurcation occurs and the emerging phytoplankton spectrum develops additional low frequency energy indicative of chaos. The *Z-only case* looks functionally similar to that of the total phytoplankton. For the most part, the *R+Z* case looks like a superposition of the *R-only* and *Z-only* cases with more broadband low frequency energy emerging across a range of forcing periods. One notable exception is for forcing periods that exceed 1000 days. Whereas the *R-only* case in this regime had an emerging band of low frequencies, this is not present in the *R+Z* case. It appears that for low forcing frequencies — lower than the individual phytoplankton's R-oscillation frequency — the Z-oscillations do not strongly interact with the R-oscillations, and they simply coexist.

A common theme in most of the above cases is that the effect of the forcing on the emerging dynamics depends on how frequency of the forcing compares with those of the intrinsic mechanisms. In the *Z-only* and *R+Z* cases for the total phytoplankton, there

is a significant region of low frequency (interannual) energy whenever the external forcing oscillates at a frequency similar to the Z-oscillations. When the external forcing is slower than the Z-oscillations, the interannual variability is reduced. The same is true for the individual species. In the *R+Z* case, there is a broad region of interannual variability when the R-oscillations occur on slower time scales than the forcing. As the forcing period increases, the R-oscillations begin to follow that of the forcing, and the interannual variability is reduced. This phenomenon, where phase-locking occurs when the external forcing is slower than the intrinsic frequencies, also emerges in much simpler linear systems. In Appendix A, we introduce an equation for biomass under sinusoidal forcing that exhibits this property.

Figure 4 is similar to Figure 3, but here the forcing period is fixed at 360 days and $\tau_{\max}$ is varied (see caption for details), allowing us to see how emerging frequencies change as the system moves from an oligotrophic region, with small annual nutrient pulses, to a highly seasonal one, with strong nutrient bursts. For the total phytoplankton (top row), we see that while the forcing frequency is dominant for the full range of $\tau_{\max}$, one can observe the emergence of several regimes from secondary frequencies in the spectra. For the *R-only* case, we see that decreasing $\tau_{\max}$ to values below 0.01 day^{-1} leads to the presence of energy in interannual wavelet periods. Limiting the nutrient supply leads to longer timescales of variability in the total, driven by longer periods of succession between individual species (compare panels A and D). For the *Z-only* case, we can observe that the modes associated with Z-oscillations (high-frequencies) shifts towards the forcing frequency as $\tau_{\max}$ decreases; this is due to the weakening of predator-prey cycles when less nutrient is available in the system to sustain the phytoplankton.

The same observations about the total phytoplankton are present for the individual species P_1^s, but are much more pronounced. The *R+Z* scenario once again resembles a superposition of the *R-only* and *Z-only* cases, with some additional low frequency energy when $\tau_{\max}$ is sufficiently large. For the *R-only* case, an increase in $\tau_{\max}$ leads to a stabilization in the dominant period as a multiple of the forcing period, as expected.

4 Stochastic Forcing

Here we examine the effects on plankton population variability of more realistic, stochastically-varying dilution rates, in three cases where the dominant frequencies are (A) mostly seasonal, (B) seasonal mixed with a subseasonal band, and (C) multi-annual. We model these forcing scenarios by constructing linear combinations of Gaussian noise, centered on various frequencies. In cases A and B, these are added to a weighted sinusoidal annual forcing term. The specific form of the variable dilution rate is

$$\tau(t) = \tau_{\min} + \frac{\hat{\tau}(t) - \min_t(\hat{\tau}(t))}{\max_t(\hat{\tau}(t)) - \min_t(\hat{\tau}(t))}(\tau_{\max} - \tau_{\min}) \tag{4}$$

where $\hat{\tau}(t)$ is a time-series given by

$$\hat{\tau}(t) = w_0 \sin\left(\frac{2\pi t}{T_3}\right) + \sum_{i=1}^{4} w_i \eta_i(t; T_i, T_{i+1}). \tag{5}$$

The forcing periods are $\{T_i\}_{i=1\ldots5} = \{30, 180, 360, 720, 1800\}$ days and $\eta_i(t; T_i, T_{i+1})$ is a time-indexed standard normal distribution that is bandpass-filtered between periods T_i and T_{i+1}. The three forcing scenarios are distinguished by their choice of weights w_i, with

$$\{w_i\}_{i=0\ldots4} = \frac{1}{32}\begin{cases} \{4, 4, 14, 10, 0\} & \text{A: Mostly seasonal} \\ \{2, 10, 16, 4, 0\} & \text{B: Seasonal with subseasonal band} \\ \{0, 0, 0, 8, 24\} & \text{C: Multiannual.} \end{cases} \tag{6}$$

Note that the weights obey the constraint $\sum_{i=0}^{4} w_i = 1$.

The temporal wavelet spectra of the forcing signals corresponding to cases A through C are shown in Figure 5, panels A to C, respectively. The middle and lower rows show the stacked wavelet spectra for simulations of the ecosystem model in the *R+Z* case, subjected to the three cases of stochastic variability, and for the same range of maximum dilution rates used in Figure 4 (see caption for details). Panels D and G of Figure 5 are similar to panels C and F of Figure 4, as the forcing contains primarily annual energy. In this case, we can see that the emerging frequencies and their dependence on $\tau_{\max}$ are similar, though the different shape of the forcings (one is sinusoidal, while the other is a linear combination of bandpass-filtered stochastic terms that are scaled between $\tau_{\min}$ and $\tau_{\max}$) introduces some discrepancies in the spectra. In general, for the total phytoplankton, an increase in the $\tau_{\max}$ leads to an increase in the dominant subseasonal frequency. Values of $\tau_{\max}$ less than 0.02 day^{-1} produce a distinct low frequency oscillation whose frequency decreases as $\tau_{\max}$ decreases.

For the individual phytoplankton P_1^s, the mostly-annual stochastic case is again similar to the annual sinusoidal case, but the dominant frequency tends to vary more smoothly with $\tau_{\max}$ in the stochastic case compared with the sinusoidal case. In the sinusoidal case, for $\tau_{\max} > 0.02$, the dominant period shifts between harmonics of the forcing period as $\tau_{\max}$ increases. In the stochastic case, the harmonics are still present, but the dominant period follows a smoother trajectory. The stochastic noise may act as a stabilizing factor to reduce the parameter sensitivity, but the two plots tell largely the same story.

The spectra that emerge in the case with significant annual and subseasonal noise are not so different from those in the mostly-annual case. The additional subseasonal noise leads to a strengthening of the non-annual frequencies (both the high frequency Z-oscillations and the low frequency oscillations that appear for smaller values of $\tau_{\max}$). But in both cases the same dominant frequencies are active and vary in the same manner with $\tau_{\max}$. As for the multiannual case, the low frequency oscillations seen in the previous two cases are present, albeit while sharing considerable overlap with the forcing frequencies. The high frequency Z-oscillations remain intact when the nutrient supply is sufficient, but these are suppressed for a small enough value of $\tau_{\max}$; this represents an oligotrophic region with slow changes in nutrient supply, and the zooplankton cannot be sustained.

In all three cases for the individual phytoplankton, the dominant emerging frequency follows a curve that increases with $\tau_{\max}$ and then asymptotes at a wavelet period of roughly 1000 days. There is also significant energy at the highest wavelet periods, indicative of low frequency aperiodicity in the system. In the multiannual case, the dominant curve is quite noisy and broadband, especially for values of $\tau_{\max}$ at or above 0.02 day^{-1}. This appears to be driven by interactions between the forcing and R-oscillations, which occur on roughly the same timescale. This noise is not present in the mostly-annual case, and is present to a much lesser degree in the annual/subseasonal case. The takeaway from these results is that both the total and individual phytoplankton in the full *R+Z* model exhibit variability over a consistent set of dominant frequencies in a variety of scenarios, with and without noise. Furthermore, these emerging frequencies align with the intrinsic mechanisms that generate them — R-oscillations for the individual species, and both R- and Z-oscillations for the total. The individual phytoplankton exhibit significant interannual variability in all cases, but the spectrum also greatly depends on the on the frequency ranges of the forcings. This implies that the community composition can vary strongly year-to-year, but it depends on both the amount of nutrient available year-round and the dominant frequencies of this nutrient supply.

5 Varying Light

In the real ocean, light and nutrient supply are often anti-correlated, especially in highly seasonal regions such as the North Atlantic. To check the robustness of our results, here we present an additional experiment with plankton growth rates limited by light, and varying both light and dilution rate in an idealized fashion representative of a high-latitude bloom, following the series C simulations of Lévy (2015). The effects of light are parameterized by multiplying μ^s and μ^l in equations 1a, 1b and 1c by $I(t)$, specified as

$$I(t) = 0.3 + 0.7\frac{e^{1-r(t)}-1}{e-1}, \quad \text{where} \quad r(t) = \begin{cases} \frac{t+60}{120} & 0 \le t < 60 \text{ days} \\ \frac{90-t}{30} & 60 \le t < 90 \text{ days} \\ 0 & 90 \le t < 300 \text{ days} \\ \frac{t-300}{120} & 300 \le t < 360 \text{ days} \end{cases} \tag{7}$$

is a ramp function that mimics mixed layer deepening and shoaling. The dilution rate in this experiment is $\tau(t) = 0.01 + 0.03r(t)$.

Figure 6 shows the forcing structures (panel A) and the individual and total wavelet spectra (panel B) for the $R{+}Z$ case when subjected to the highly seasonal forcing scenario above. We observe that the high frequency variability seen in the previous simulations is preserved, for both the individual and total phytoplankton. But the low frequency, interannual variability is only preserved in the individual species spectra. Additional work should be done to incorporate light as another dimension in parameter space. But we expect that the results in this study will translate even to highly seasonal cases with variable light.

6 Discussion and Conclusion

In this study, we have explored how interactions between extrinsic and intrinsic variability might influence the dynamics of a phytoplanktonic ecosystem by using a biogeochemical model with time-varying forcings. We found that the emerging frequencies in the total biomass depend on the timescale of the forcing relative to that of the intrinsic frequency. When the forcing period is on the same order as the intrinsic period, the intrinsic frequencies remain dominant. When the forcing period is longer than the intrinsic period, then the ecosystem exhibits stronger phase-locking to this extrinsic period, but typically retains any existing predator-prey cycles. Low-amplitude nutrient fluctuations tend to produce low frequency variability, especially at the individual level, indicating slower timescales of community evolution. These observations hold under both deterministic and forcings with stochastic noise.

We can use these results to revisit the questions that posed earlier in the study. First, are intrinsic oscillations typically eliminated in the presence of extrinsic variability? Or do the frequencies associated with the intrinsic and extrinsic mechanisms coexist? Our results primarily support coexistence. Intrinsic variability is typically robust to the external variability we impose. The exception is under low-amplitude, low-frequency nutrient fluctuations, where phytoplankton are not sustained at sufficient levels of biomass to enable predator-prey oscillations. Second, do the interactions between the sources of variability produce previously unseen frequencies? Our observation, which is most plainly visible from Figure 2, is that extrinsic and intrinsic variability can interact to produce strong interannual variability that is uncharacteristic of either component in isolation. This happens when the forcing occurs on an intraseasonal-seasonal timescale. This lines up with the hypothesis of Dakos et al. (2009) that interannual variability could emerge from ecological interactions in diverse communities even under regular (seasonal) forcing.

Our results indicate that intrinsic variability is not necessarily dwarfed by external forcings, and the two may work in concert to produce the wide variety of timescales observed in phytoplankton time series. We expect that both regional differences in nutrient availability (in magnitude and frequency of delivery) and ecological community structure will play a role in shaping the observed variability in phytoplankton time series. This is an important factor to consider when working with climate projection models, as climate change will impact sources of variability that are both extrinsic and intrinsic to planktonic communities. Of course, more work needs to be done to better understand the interplay between intrinsic and extrinsic variability. In particular, our physical framework only includes temporal variations in nutrient supply, without considering light or any spatial variability. In Section 5 we demonstrated a short experiment that confirms intrinsic variability should persist in the presence of light variations, but much more work remains to be done. We hope to introduce a more complex physical model in a future study.

7 Open Research

The ecosystem model (Mayersohn & Mangolte, 2022) is a modified version of the model used in Mayersohn et al. (2021) and is available on Github. It is also archived in a Zenodo repository with DOI `10.5281/zenodo.6347768`. The `waipy` wavelet package, written by Mabel Calim Costa and inspired by the work of Torrence and Compo (1998), is available in a Github repository: `https://github.com/mabelcalim/waipy`.

Acknowledgments

The authors thank Stephanie Dutkiewicz and Olivier Aumont for early feedback on this work. BM, KSS, and ML gratefully acknowledge support from the New York University Abu Dhabi Institute, through its Center for Prototype Climate Modeling. ML gratefully acknowledges support from TOSCA-CNES and ANR-SOBUMS (contract ANR-16-CE01-0014).

References

Alvain, S., Moulin, C., Dandonneau, Y., & Loisel, H. (2008). Seasonal distribution and succession of dominant phytoplankton groups in the global ocean : A satellite view. *Global Biogeochemical Cycles*, *22*(July), 1–15. doi: 10.1029/2007GB003154

Aumont, O., Maury, O., Lefort, S., & Bopp, L. (2018). Evaluating the Potential Impacts of the Diurnal Vertical Migration by Marine Organisms on Marine Biogeochemistry. *Global Biogeochemical Cycles*, *32*(11), 1622–1643. doi: 10.1029/2018GB005886

Aumont, O., Tagliabue, A., Bopp, L., & Gehlen, M. (2015). PISCES-v2 : an ocean biogeochemical model for carbon and ecosystem studies. *Geoscientific Model Development*, *8*(1990), 2465–2513. doi: 10.5194/gmd-8-2465-2015

Behrenfeld, M. J., O'Malley, R. T., Siegel, D. A., McClain, C. R., Sarmiento, J. L., Feldman, G. C., ... Boss, E. S. (2006). Climate-driven trends in contemporary ocean productivity. *Nature*, *444*(7120), 752–755. doi: 10.1038/nature05317

Benincà, E., Huisman, J., Heerkloss, R., Johnk, K. D., Branco, P., Van Nes, E. H., ... Ellner, S. P. (2008). Chaos in a long-term experiment with a plankton community. *Nature Letters*, *451*(February). doi: 10.1038/nature06512

Blasius, B., Rudolf, L., Weithoff, G., Gaedke, U., & Fussmann, G. F. (2019). Long-term cyclic persistence and phase signature in an experimental predator-prey system. *Nature*(July), 1–36. Retrieved from `http://dx.doi.org/10.1038/s41586-019-1857-0` doi: 10.1038/nature11356

Carranza, M. M., & Gille, S. T. (2014). Southern Ocean wind-driven entrainment enhances satellite chlorophyll-a through the summer. *Journal of Geophysical Research: Oceans*, 2121–2128. doi: 10.1002/jgrc.20224

Chavez, F. P., Messi, M., & Pennington, J. T. (2011). Marine Primary Production in Relation to Climate Variability and Change. *Annu. Rev. Mar. Sci.*, *3*, 227–260. doi: 10.1146/annurev.marine.010908.163917

Dakos, V., Benincà, E., Van Nes, E. H., Philippart, C. J. M., Scheffer, M., & Huisman, J. (2009). Interannual variability in species composition explained as seasonally entrained chaos. *Proceedings of the Royal Society B: Biological Sciences*, *276*(1669), 2871–2880. doi: 10.1098/rspb.2009.0584

Demarcq, H., Reygondeau, G., Alvain, S., & Vantrepotte, V. (2012). Monitoring marine phytoplankton seasonality from space. *Remote Sensing of Environment*, *117*, 211–222. Retrieved from `http://dx.doi.org/10.1016/j.rse.2011.09.019` doi: 10.1016/j.rse.2011.09.019

D'Ovidio, F., De Monte, S., Alvain, S., Dandonneau, Y., & Lévy, M. (2010). Fluid dynamical niches of phytoplankton types. *Proceedings of the National Academy of Sciences of the United States of America*, *107*(43), 18366–18370. doi: 10.1073/pnas.1004620107

Dutkiewicz, S., Hickman, A. E., Jahn, O., Henson, S., Beaulieu, C., & Monier, E. (2019). Ocean colour signature of climate change. *Nature Communications*, *10*(1). Retrieved from `http://dx.doi.org/10.1038/s41467-019-08457-x` doi: 10.1038/s41467-019-08457-x

Edwards, A. M. (2001, 4). Adding Detritus to a Nutrient-Phytoplankton-Zooplankton Model:A Dynamical-Systems Approach. *Journal of Plankton Research*, *23*(4), 389–413. Retrieved from `http://plankt.oxfordjournals.org/content/23/4/389.full` doi: 10.1093/plankt/23.4.389

Fauchereau, N., Tagliabue, A., Bopp, L., & Monteiro, P. M. (2011). The response of phytoplankton biomass to transient mixing events in the Southern Ocean. *Geophysical Research Letters*, *38*(17), 1–6. doi: 10.1029/2011GL048498

Follows, M. J., Dutkiewicz, S., Grant, S., & Chisholm, S. W. (2007). Emergent biogeography of microbial communities in a model ocean. *Science (New York, N.Y.)*, *315*(5820), 1843–1846. Retrieved from `http://www.ncbi.nlm.nih.gov/pubmed/17395828` doi: 10.1126/science.1138544

Harris, G. P., & Baxter, G. (1996). Interannual variability in phytoplankton biomass and species composition in a subtropical reservoir. *Freshwater Biology*, *35*(3), 545–560. doi: 10.1111/j.1365-2427.1996.tb01768.x

Hastings, A. (2020, jan). *Long-term predator-prey cycles finally achieved in the lab* (Vol. 577) (No. 7789). NLM (Medline). doi: 10.1038/d41586-019-03603-3

Heerkloss, R., & Klinkenberg, G. (1998, 5). A long-term series of a planktonic foodweb: a case of chaotic dynamics. *SIL Proceedings, 1922-2010*, *26*(4), 1952–1956. doi: 10.1080/03680770.1995.11901083

Hsieh, C. H., Glaser, S. M., Lucas, A. J., & Sugihara, G. (2005). Distinguishing random environmental fluctuations from ecological catastrophes for the North Pacific Ocean. *Nature*, *435*(7040), 336–340. doi: 10.1038/nature03553

Huisman, J., Pham Thi, N. N., Karl, D. M., & Sommeijer, B. (2006). Reduced mixing generates oscillations and chaos in the oceanic deep chlorophyll maximum. *Nature*, *439*(7074), 322–325. doi: 10.1038/nature04245

Huisman, J., van Oostveen, P., & Weissing, F. J. (1999). Critical depth and critical turbulence: Two different mechanisms for the development of phytoplankton blooms. *Limnology and Oceanography*, *44*(7), 1781–1787.

Huisman, J., & Weissing, F. J. (1999). Biodiversity of plankton by species oscillations and chaos. *Nature*, *402*(6760), 407–410. doi: 10.1038/46540

Keerthi, M. G., Levy, M., Aumont, O., Lengaigne, M., & Antoine, D. (2020, may). Contrasted Contribution of Intraseasonal Time Scales to Surface Chlorophyll Variations in a Bloom and an Oligotrophic Regime. *Journal of Geophysical*

Research: Oceans, *125*(5). doi: 10.1029/2019jc015701

Lévy, M. (2015). Exploration of the critical depth hypothesis with a simple NPZ model. *ICES Journal of Marine ScienceMarine Science*, *72*(January), 1916–1925.

Lévy, M., Franks, P. J., & Smith, K. S. (2018). The role of submesoscale currents in structuring marine ecosystems. *Nature communications*, *9*(1), 4758. doi: 10.1038/s41467-018-07059-3

Mahadevan, A., D'Asaro, E., Lee, C., & Perry, M. J. (2012, jul). Eddy-driven stratification initiates North Atlantic spring phytoplankton blooms. *Science (New York, N.Y.)*, *337*(6090), 54–58. Retrieved from `http://www.sciencemag.org/content/337/6090/54.abstract` doi: 10.1126/science.1218740

Martinez, E., Antoine, D., Ortenzio, F. D., & Gentili, B. (2009). Climate-Driven Basin-Scale Decadal Oscillations of Oceanic Phytoplankton. *Science*, *1253*(November). doi: 10.1126/science.1177012

Mayersohn, B., & Mangolte, I. (2022). *PHYtoplankton-REsource (and Zooplankton) model [Software]. Zenodo.* Retrieved from `https://doi.org/10.5281/zenodo.6347768` doi: 10.5281/zenodo.6347768

Mayersohn, B., Smith, K. S., Mangolte, I., & Lévy, M. (2021). Intrinsic timescales of variability in a marine plankton model. *Ecological Modelling*, *443*(July 2020), 109446. Retrieved from `https://doi.org/10.1016/j.ecolmodel.2021.109446` doi: 10.1016/j.ecolmodel.2021.109446

Mayot, N., D'Ortenzio, F., Uitz, J., Gentili, B., Ras, J., Vellucci, V., ... Claustre, H. (2017). Influence of the Phytoplankton Community Structure on the Spring and Annual Primary Production in the Northwestern Mediterranean Sea. *Journal of Geophysical Research: Oceans*, *122*(12), 9918–9936. doi: 10.1002/2016JC012668

Menkes, C. E., Lengaigne, M., Lévy, M., Ethé, C., Bopp, L., Aumont, O., ... Jullien, S. (2016). Global impact of tropical cyclones on primary production. *Global Biogeochemical Cycles*, *29*, 767–786. doi: 10.1002/2015GB005214.Received

Messié, M., & Chavez, F. P. (2017). Nutrient supply, surface currents, and plankton dynamics predict zooplankton hotspots in coastal upwelling systems. *Geophysical Research Letters*, *44*(17), 8979–8986. Retrieved from `https://onlinelibrary.wiley.com/doi/full/10.1002/2017GL074322` doi: 10.1002/2017GL074322

Messié, M., Ledesma, J., Kolber, D. D., Michisaki, R. P., Foley, D. G., & Chavez, F. P. (2009). Progress in Oceanography Potential new production estimates in four eastern boundary upwelling ecosystems. *Progress in Oceanography*, *83*(1-4), 151–158. Retrieved from `http://dx.doi.org/10.1016/j.pocean.2009.07.018` doi: 10.1016/j.pocean.2009.07.018

Millman, K. J., & Aivazis, M. (2011, mar). *Python for scientists and engineers* (Vol. 13) (No. 2). doi: 10.1109/MCSE.2011.36

Poggiale, J., Eynaud, Y., & Baklouti, M. (2013). Impact of periodic nutrient input rate on trophic chain properties. *Ecological Complexity*, *14*, 56–63. Retrieved from `http://dx.doi.org/10.1016/j.ecocom.2013.01.005` doi: 10.1016/j.ecocom.2013.01.005

Redfield, A. C. (1934). *On the proportions of organic derivatives in sea water and their relation to the composition of plankton.* University Press of Liverpool.

Resplandy, L., Vialard, J., Lévy, M., Aumont, O., & Dandonneau, Y. (2009). Seasonal and intraseasonal biogeochemical variability in the thermocline ridge of the southern tropical Indian Ocean. *Journal of Geophysical Research: Oceans*, *114*(7), 1–13. doi: 10.1029/2008JC005246

Rousseaux, C. S., & Gregg, W. W. (2015). Recent decadal trends in global phytoplankton composition. *Global Biogeochemical Cycles*, 1674–1688. doi: 10.1002/2015GB005139.Received

Salgado-Hernanz, P. M., Racault, M. F., Font-Muñoz, J. S., & Basterretxea, G. (2019). Trends in phytoplankton phenology in the Mediterranean Sea based on ocean-colour remote sensing. *Remote Sensing of Environment*, *221*(November 2018), 50–64. Retrieved from `https://doi.org/10.1016/j.rse.2018.10.036` doi: 10.1016/j.rse.2018.10.036

Smayda, T. J. (1998). Patterns of variability characterizing marine phytoplankton, with examples from Narragansett Bay. *ICES Journal of Marine Science*, *55*(4), 562–573. doi: 10.1006/jmsc.1998.0385

Sugihara, G., & May, R. M. (1990). Nonlinear forecasting as a way of distinguishing chaos from measurement error in time series. *Nature*, *344*(April), 24–26.

Sverdrup, H. U. (1953). On conditions for the vernal blooming of phytoplankton. *ICES Journal of Marine Science*, *18*(3), 287–295. doi: 10.1093/icesjms/18.3.287

Talling, J. F. (1993). Comparative seasonal changes, and inter-annual variability and stability, in a 26-year record of total phytoplankton biomass in four English lake basins. *Hydrobiologia*, *268*(2), 65–98. doi: 10.1007/BF00006879

Taylor, J. R., & Ferrari, R. (2011). Shutdown of turbulent convection as a new criterion for the onset of spring phytoplankton blooms. *Limnology and Oceanography*, *56*(6), 2293–2307. doi: 10.4319/lo.2011.56.6.2293

Thomalla, S. J., Fauchereau, N., Swart, S., & Monteiro, P. M. (2011). Regional scale characteristics of the seasonal cycle of chlorophyll in the Southern Ocean. *Biogeosciences*, *8*(10), 2849–2866. doi: 10.5194/bg-8-2849-2011

Tilman, D. (1985). The Resource-Ratio Hypothesis of Plant Succession. *The American Naturalist*, *125*(6), 827–852.

Torrence, C., & Compo, G. P. (1998). A Practical Guide to Wavelet Analysis. *Bulletin of the American Meteorological Society*, *79*(1), 61–78. doi: 10.1175/1520-0477(1998)079⟨0061:APGTWA⟩2.0.CO;2

Vantrepotte, V., & Mélin, F. (2011). Inter-annual variations in the SeaWiFS global chlorophyll a concentration (1997-2007). *Deep-Sea Research Part I: Oceanographic Research Papers*, *58*(4), 429–441. doi: 10.1016/j.dsr.2011.02.003

8 Figures

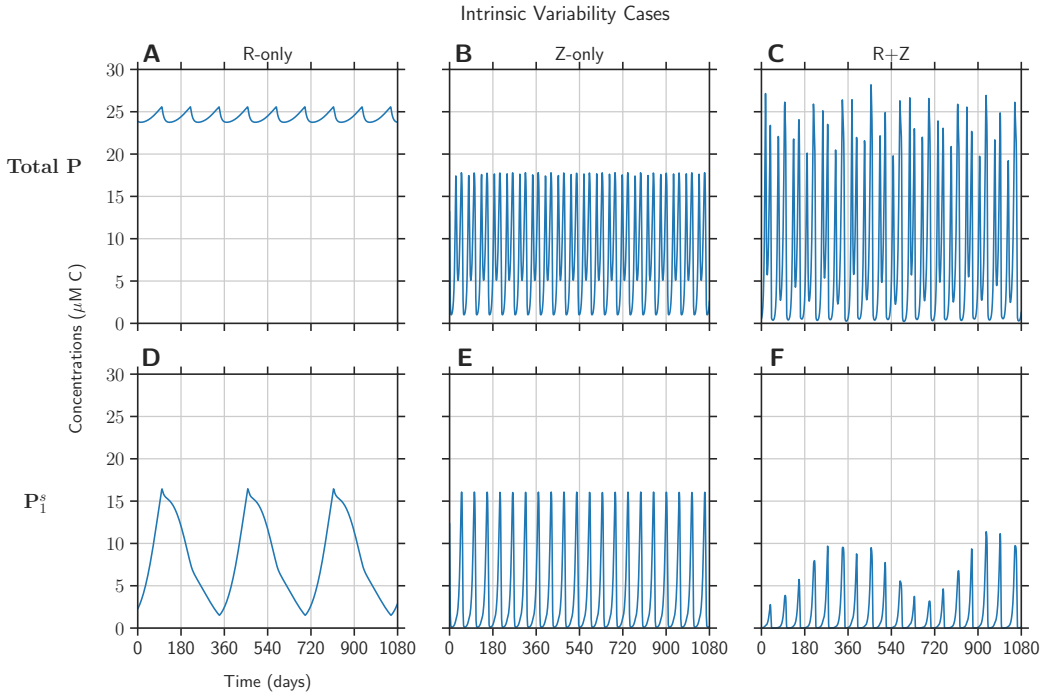

Figure 1. Three cases demonstrating intrinsic oscillations in the total phytoplankton and an individual small phytoplankton P_1^s: Oscillations generated by competition for resources, or R-oscillations (*R-only*); predator-prey oscillations between zooplankton and phytoplankton, or Z-oscillations (*Z-only*); and both kinds of oscillations (*R+Z*). The dilution rate (τ) is set to a constant value of 0.04 day^{-1}, which is typical of an upwelling region (Messié et al., 2009). The other parameter values correspond to the strong predation case of Mayersohn et al. (2021).

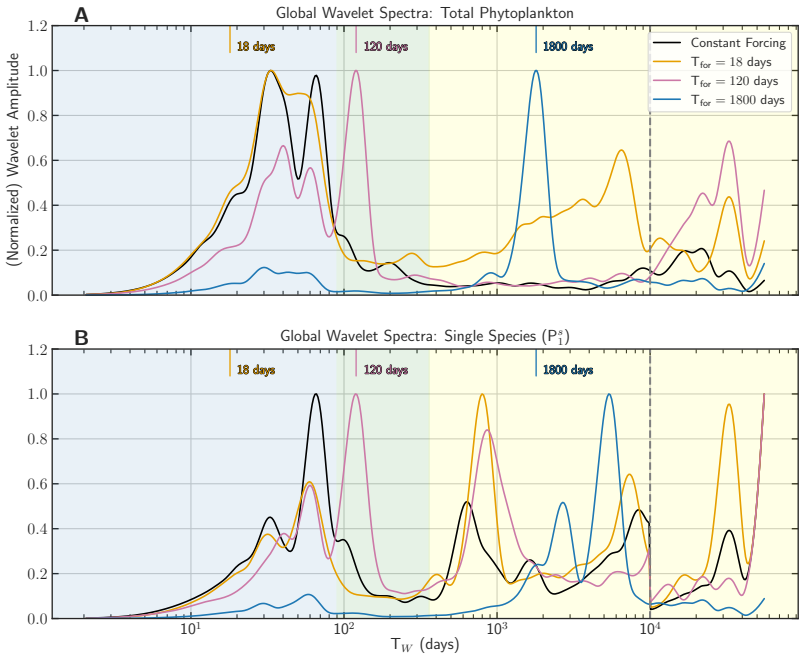

Figure 2. Global wavelet spectra of total phytoplankton (top row) and a single species P_1^s (bottom row) for sinusoidally-varying dilution rates, with $\tau_{\min} = 0$ day^{-1}, $\tau_{\max} = 0.04$ day^{-1}, and forcing periods $T_{\text{for}} = 18, 120, 1800$ days. Also shown is a case with constant dilution rate $\tau = 0.04$ day^{-1}. Intraseasonal, near-annual, and multiannual variability is indicated by the blue, green, and yellow shadings, respectively. Wavelet periods to the right of the vertical gray dashed line fall within the wavelet transform's "cone of influence", which means that they are potentially distorted by boundary effects. Curves that achieve their maximum value within the cone of influence are normalized in two parts — one to the left of the dashed line and the other to the right — in order to ensure significant emerging periods are not overwhelmed by artifacts of the transform.

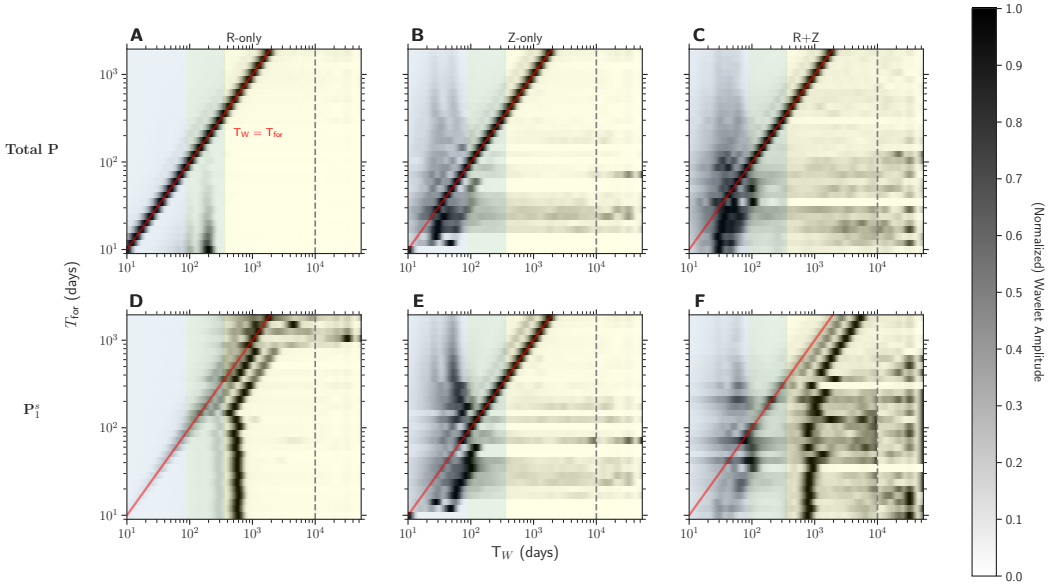

Figure 3. Wavelet spectra of the total phytoplankton (panels A-C) and individual phytoplankton (panels D-F) for forcing periods T_{for} ranging across 30 logarithmically-spaced (rounded to the nearest day) values between 10 days^{-1} and 1800 days^{-1}, with 10 additional values at key periods of 30, 90, 120, 180, 270, 360, 540, 720, 1080, and 1440 days. The maximum dilution rate $\tau_{\max} = 0.04$ day^{-1} and the minimum dilution rate $\tau_{\min} = 0$ day^{-1}. Each row represents the normalized wavelet spectrum of a single simulation: the grayscale represents the wavelet amplitude and the x-axis is the wavelet period. The spectra of these individual simulations are stacked vertically in increasing order of the sweep parameter value. For each value of the sweep parameter, we normalize the square root of the wavelet spectrum between 0 and 1. The meaning of the vertical gray dashed line is explained in the caption of Figure 2.

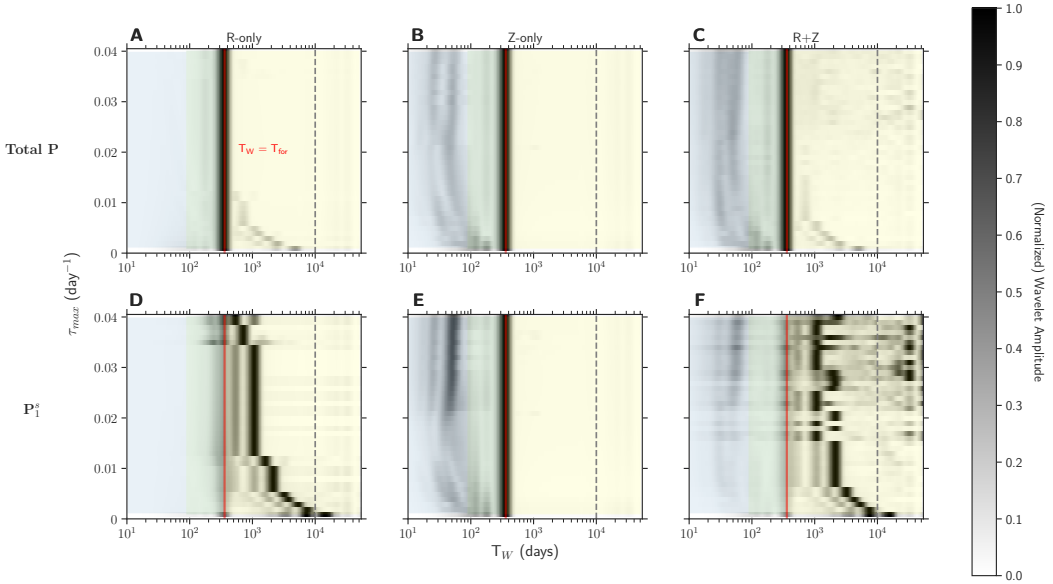

Figure 4. Wavelet spectra of the total phytoplankton (panels A-C) and individual phytoplankton (panels D-F) for maximum dilution rates $\tau_{\max}$ ranging across 40 linearly-spaced values between 0 day^{-1} and 0.04 day^{-1}. The forcing period $T_{\text{for}} = 360$ days and the minimum dilution rate $\tau_{\min} = 0$ day^{-1}. Each row represents the normalized wavelet spectrum of a single simulation: the grayscale represents the wavelet amplitude and the x-axis is the wavelet period. The spectra of these individual simulations are stacked vertically in increasing order of the sweep parameter value. For each value of the sweep parameter, we normalize the square root of the wavelet spectrum between 0 and 1. The meaning of the vertical gray dashed line is explained in the caption of Figure 2.

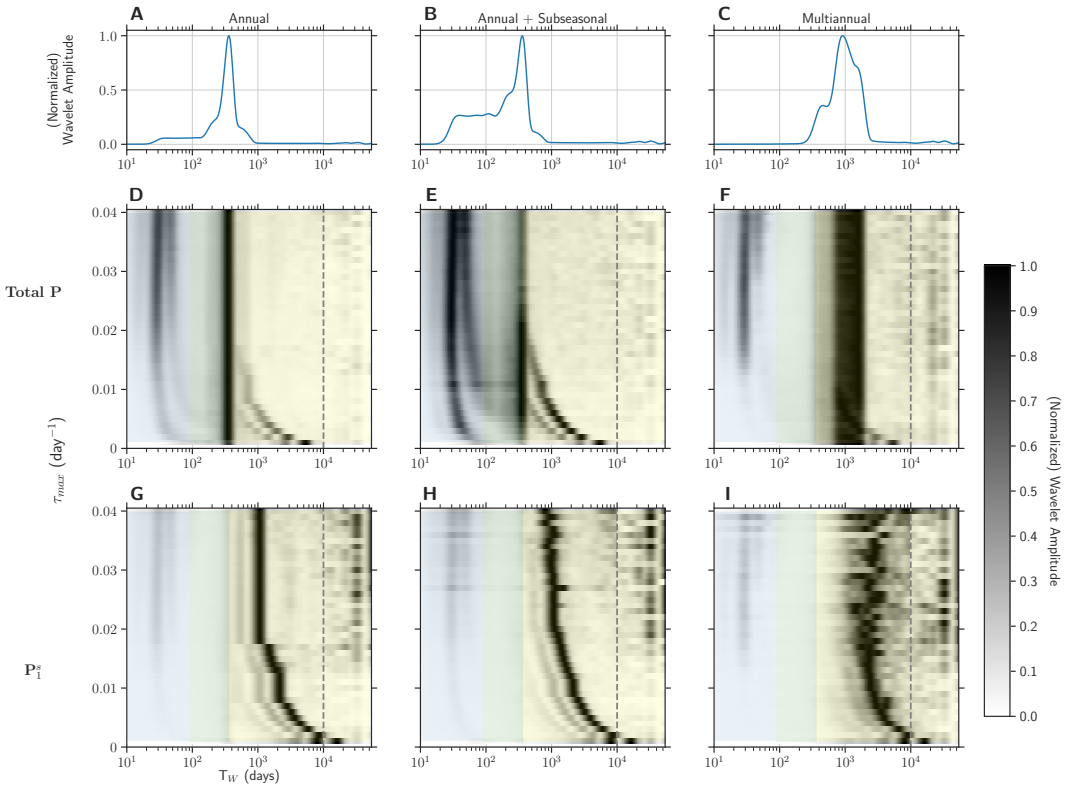

Figure 5. Normalized wavelet spectra for the R+Z ecosystem subjected to stochastically-generated forcings, with $\tau_{\min} = 0$ day^{-1} and $\tau_{\max}$ ranging across 40 linearly-spaced values between 0 day^{-1} and 0.04 day^{-1}. The top row shows the forcing spectra, which correspond to predominantly annual (A), strong annual and subseasonal components (B), and predominantly multiannual (C) frequencies, corresponding to entries in Table 4. The bottom two rows show normalized spectra of total phytoplankton (D-F) and individual phytoplankton P_1^s (G-I). The grayscale represents the wavelet amplitude and the x-axis is the wavelet period T_W. The spectra of these individual simulations are stacked vertically in increasing order of the sweep parameter value. For each value of the sweep parameter, we normalize the square root of the wavelet spectrum between 0 and 1. The meaning of the vertical gray dashed line is explained in the caption of Figure 2.

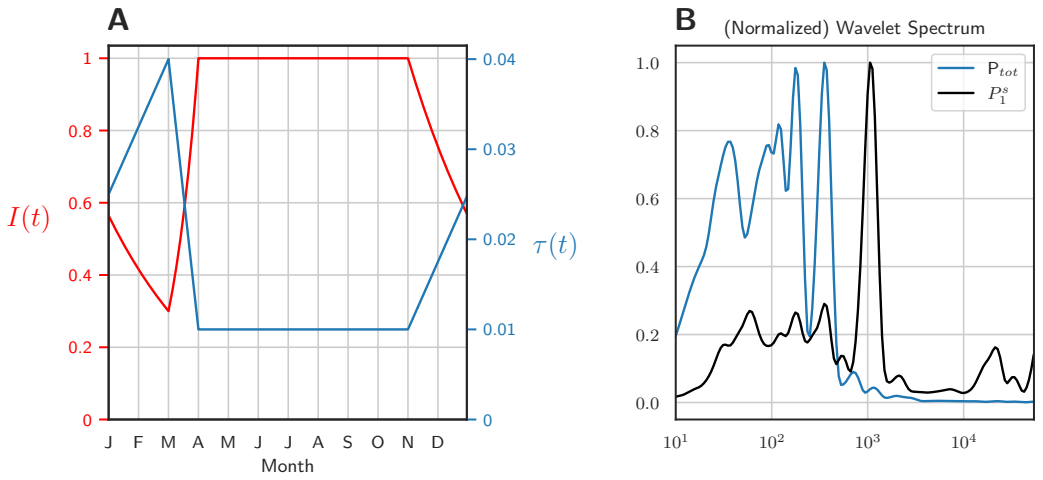

Figure 6. Global wavelet spectra of total phytoplankton and individual phytoplankton biomass (panel B) in a simulated ecosystem in the *R+Z* scenario, subjected to seasonally-varying light and nutrient supply (panel A), characteristic of highly seasonal regions such as the North Atlantic Ocean. The total phytoplankton exhibits a strong annual peak, along with subseasonal variability typical of Z-oscillations. The interannual component seen for some simulations is not present. The individual phytoplankton most strongly oscillates at a period three times that of the annual peak due to the cycle in species composition between blooms. A strong interannual component remains, indicating that the addition of seasonality in light still permits chaotic/aperiodic changes in species composition.

9 Tables

Parameter	Value	Units	Description
S_j	18.1, 1.21, 1.21×10^{-3}	$[R_j]$	Deep nutrient source values[1]
μ^s, μ^l	0.308, 0.616	day^{-1}	Maximum phytoplankton growth rates[2]
m_P	0.1	day^{-1}	Phytoplankton mortality rate[2]
r_j	0.15, 0.01, 1×10^{-5}	$\frac{[R_j]}{\mu\text{M C}}$	Nutrient : Carbon ratios[3]
$c_{\min}, c_{\max}$	0.9, 1.3		Stoichiometric scaling factors
$\kappa_j^s = \frac{1}{4}\kappa_j^l$	0.15, 0.01, 1×10^{-5}	$[R_j]$	Nutrient uptake half-saturation constants[2]
$k_{\min}, k_{\max}$	0.7, 1.1		Nutrient half-saturation scaling factors
g^s, g^l	1.5, 0.5	day^{-1}	Grazing rates[4]
K_Z	10	μM C	Grazing half-saturation constant[4]
m_Z	0.015	$(\mu\text{M C} \cdot \text{day})^{-1}$	Zooplankton mortality rate[5]

[1] Messié et al. (2009)
[2] Follows et al. (2007)
[3] r_1 = N:C, r_2 = PO_4:C, r_3 = Fe:C (Redfield, 1934)
[4] Aumont et al. (2015)
[5] Messié and Chavez (2017)

Table 1. Definitions and default values for model parameters. Subscript j = 1,2,3. The notation $[R_j]$ means 'the units of R_j', which are $[R_1] = \mu$M N, $[R_2] = \mu$M PO_4, and $[R_3] = \mu$M Fe. References for default values are given where appropriate in footnotes.

Appendix A First-Order Autoregressive Biomass Equation

We observed in Figure 3 in Section 3 that a bifurcation occurred when the forcing period T_{for} began to exceed the dominant intrinsic period in the system. When the forcing period increased, the emerging wavelet period became locked to that of the forcing. When the forcing period decreased, the intrinsic period dominated the emerging spectrum. This relationship can also be found in much simpler linear systems. Consider an equation for biomass $C(t)$ that responds to external forcing with a fixed response rate γ. The external forcing $C_{\text{forcing}}(t)$ fluctuates sinusoidally at a frequency f. The optimal value of C at any given time is $C_{\text{forcing}}(t)$, but C is limited by the rate γ at which it can respond to this forcing. The equations are

$$\frac{\mathrm{d}C}{\mathrm{d}t} = \gamma\left[C_{\text{forcing}}(t) - C\right] \quad \text{where} \quad C_{\text{forcing}}(t) = C_0\left[1 + \sin\left(ft\right)\right]$$

The solution to this equation is

$$C = \frac{C_0}{\gamma^2 + f^2}\left[\gamma^2(1 + \sin(ft)) - f\gamma\cos(ft) + f^2\right] + A\exp(-\gamma t)$$

where A depends on the initial value of C. The initial condition becomes less relevant as $t \to \infty$, and there exist two main outcomes depending on the relative values of γ and f:

1. If $f \gg \gamma$, C cannot respond quickly enough to the fluctuations, and as $f \to \infty$, the solution approaches C_0. Thus the external forcing loses its influence if it is too fast.
2. If $f \ll \gamma$, then the solution approaches $C_0[1 + \sin(ft)] = C_{\text{forcing}}(t)$. In other words, the solution phase locks to the external forcing.

Our ecosystem model contains many additional complexities that are not captured by this simple system, but the influence of the forcing period on the emerging wavelet period is captured by this heuristic model.